Genetic Clustering on the Hippocampal Surface for Genome-Wide Association Studies

Derrek P. Hibar[1], Sarah E. Medland[2], Jason L. Stein[1], Sungeun Kim[3], Li Shen[3],
Andrew J. Saykin[3], Greig I. de Zubicaray[4], Katie L. McMahon[5],
Grant W. Montgomery[2], Nicholas G. Martin[2], Margaret J. Wright[2], Srdjan Djurovic[6],
Ingrid A. Agartz[6,7], Ole A. Andreassen[6], and Paul M. Thompson[1]

[1] Imaging Genetics Center, Laboratory of Neuro Imaging,
UCLA School of Medicine, Los Angeles, CA, USA
[2] Queensland Institute of Medical Research, Brisbane, Australia
[3] Center for Neuroimaging, Department of Radiology and Imaging Sciences,
Indiana University School of Medicine, Indianapolis, IN, USA
[4] Functional Magnetic Resonance Imaging Laboratory, School of Psychology,
University of Queensland, Brisbane, Australia
[5] Centre for Advanced Imaging, University of Queensland, Brisbane, Queensland, Australia
[6] KG Jebsen Centre for Psychosis Research, Institute of Clinical Medicine,
University of Oslo, Oslo, Norway
[7] Department of Psychiatry, Diakonhjemmet Hospital, Oslo, Norway

Abstract. Imaging genetics aims to discover how variants in the human genome influence brain measures derived from images. Genome-wide association scans (GWAS) can screen the genome for common differences in our DNA that relate to brain measures. In small samples, GWAS has low power as individual gene effects are weak and one must also correct for multiple comparisons across the genome and the image. Here we extend recent work on genetic clustering of images, to analyze surface-based models of anatomy using GWAS. We performed spherical harmonic analysis of hippocampal surfaces, automatically extracted from brain MRI scans of 1254 subjects. We clustered hippocampal surface regions with common genetic influences by examining genetic correlations (r_g) between the normalized deformation values at all pairs of surface points. Using genetic correlations to cluster surface measures, we were able to boost effect sizes for genetic associations, compared to clustering with traditional phenotypic correlations using Pearson's r.

Keywords: heritability, GWAS, clustering, hippocampus, 3D surfaces, imaging genetics.

1   Introduction

An important focus of biomedical research is the analysis of biomarkers – easily attainable and reproducible measurements that relate to disease severity or predict clinical decline. In neuroimaging, methods that quantify brain morphometry (e.g., anatomical volumes or shapes, expansions, contractions, etc.) offer promising biomarkers for a

variety of brain diseases and disorders. Surface-based morphometry of cortical and subcortical structures has been greatly advanced by ideas in computational geometry – many groups have applied surface meshes, "*M*-reps", spectral analysis, differential forms, or partial differential equations – to map disease effects and dynamic changes in the brain [1]. Surface models of subcortical structures such as the hippocampus can reveal 3D shape differences between healthy controls and patients with neurological or psychiatric disorders such as schizophrenia [2] and Alzheimer's disease [3].

More recently, researchers in *imaging genetics* have adapted computational anatomy methods to analyze genetic effects on the brain. Many brain diseases are genetically influenced, and there is an urgent need to find specific variants in our DNA – both common and rare – that contribute to variations in disease and brain measures. It is now feasible to test how variants along the human genome relate to disease biomarkers or imaging measures using genome-wide association scans (GWAS). One study recently applied GWAS to brain MRI data from over 21,000 people, discovering new genetic variants affecting hippocampal volumes [4]. However, GWA studies have low power if they test a large number of individual phenotypes – if GWAS is run at each voxel in an image, an astronomical correction must be made for the multiple statistical tests across the image and genome [5,6]. Here we build on recent work [7,8] using genetic clustering to increase power and prioritize regions for GWAS. We develop a framework to perform GWAS on 3D anatomical surface models. We demonstrate our method on hippocampal surfaces from a large cohort of 1254 subjects, scanned in independent studies on 3 continents.

2   Methods

2.1   Imaging Data

3D T1-weighted structural brain MRI and genotyping data were obtained from three independent cohorts: the Alzheimer's Disease Neuroimaging Initiative (ADNI), Queensland Twins Imaging Study (QTIM), and Thematically Organized Psychosis Study (TOP). We focused on healthy controls from each study, but we also included people with mild cognitive impairment (MCI) in the ADNI. In total, there were 511 ADNI subjects (299 males; age mean±sd: 75.5±6.5 years; 323 MCI patients), 571 QTIM subjects (218 males; age mean±sd: 23.9±2.3 years; monozygotic and dizygotic twins and siblings from 335 families), and 172 TOP subjects (90 males; age mean±sd: 35.8±9.8). Genotyping data was filtered to remove SNPs with minor allele frequency <0.01, call rate <95%, violations of Hardy-Weinberg Equilibrium $p<1 \times 10^{-6}$. The filtered genotype data was imputed to a custom '1000 Genomes' reference set (phase 1, release 3) which excludes non-European samples and singleton SNPs [9].

2.2   Hippocampal Surface Generation

Hippocampal (HP) segmentations were obtained using the freely-available and automated FSL FIRST segmentation algorithm [10]. Segmentation quality for the left and right hippocampus across all three cohorts was individually inspected by the first author. Subjects with segmentations not covering the entire HP, or including regions outside the HP (defined by [11]) were removed. The SPHARM-MAT Toolbox for

Matlab (V1.0) [12,13] was used to generate hippocampal surface models. First, we ensured that each binary segmentation label had a spherical topology. Binary segmentations were parameterized using triangular mesh surfaces, with a bijective mapping of each point p on the surface to a unit sphere with (θ, φ) coordinates, such that:

$p(\theta, \varphi) = (x(\theta, \varphi), y(\theta, \varphi), z(\theta, \varphi))^T$, using the Control of Area and Length Distortions (CALD) algorithm [12]. The object surface was then expanded in terms of a set of spherical harmonic basis functions of order m and degree l [13]. This expansion has the form $p(\theta, \varphi) = \sum_{m=0}^{\infty} \sum_{l=-m}^{m} C_l^m Y_l^m(\theta, \varphi)$, where p is defined as above and C_l^m is a set of Fourier coefficient weights for the basis functions: $C_l^m = (c_{xl}^m, c_{yl}^m, c_{zl}^m)^T$. The spherical harmonic models of the surfaces were then aligned using 12 degrees of freedom to a common template model comprised of an average of 40 healthy controls from the QTIM sample using the SHREC algorithm [14]. A translation and rotation matrix for a given mesh to the common template using SHREC matches landmarks on the surface of an object to similar points on the template (a solution is found by minimizing the root mean squared distance) [14]. In this way, we mapped the points along the surface to a common space across subjects and studies, while preserving individual morphometric differences of interest.

2.3   Quantifying Morphometric Differences on Surfaces

We determined the distance a given point on the hippocampal surface had to be deformed to match the equivalent point on the common template surface by first calculating the simple deformation matrix, $M = (x_i, y_i, z_i)$, where i is the index of vertices of length n, from a coordinates matrix V of vertices compared to the vertices in the average template A: $M = V - A$. Next we calculated the vertex normals of each individual's 3D mesh in MATLAB using the *patch* function, which returns an n-by-3 normalization matrix, **N**. We project the deformation onto the vertex normals and obtain a vector of deformation scalars for each vertex, s, such that: $s_i = \sum_{j=1}^{3} (M \cdot N)_{i,j}$. The deformation value preserves in-out differences along the surface normal (a contraction or expansion to match the template). Each value in the normalized deformation vector, s, represents the expansion or contraction required to match a given vertex on the surface of an individual subject's hippocampal surface to the equivalent point on the average template surface.

2.4   Optimizing Parameters Using Test-Retest Data

To examine the ideal parameters required to maximize the reliability of the hippocampus surface reconstruction while minimizing data smoothing and the density of the reconstructed 3D mesh, we obtained test-retest data from 40 healthy young adults in the QTIM study scanned twice on the same scanner with a mean interval of four months. We examined how the reliability of surface reconstruction within the same subject changes, as a function of the surface sampling density and the extent of heat kernel smoothing [14]. We calculated the intraclass correlation coefficient (ICC) at each point along the surface to quantify the reproducibility of hippocampal surface models across test-retest data.

2.5   Genetic Versus Phenotypic Clustering and GWAS

We wanted to compare the GWAS performance of clustered regions of interest on the hippocampal surfaces chosen by *genetic correlation* (r_g) relative to those chosen by traditional phenotypic correlations using Pearson's r_p. We calculated the genetic and phenotypic correlations between the normalized deformation values at each point on the surface with all other deformation values on the surface bilaterally, yielding a genetic correlation matrix and a separate phenotypic correlation matrix of the same size. We calculated r_g using the cross-twin, cross-trait method in 142 dizygotic and 120 monozygotic twin pairs, controlling for age and sex [15]. The phenotypic correlation r_p was the partial correlation between traits, controlling for age and sex. The genetic correlation determines areas on the surface of the hippocampus with common genetic determinants by using the known genetic relationships between monozygotic and dizygotic twins. This is not the same as phenotypic correlations, where measures from different regions can covary due to a combination of genetic *and environmental* effects. The genetic correlation is calculated from the covariance between two traits: $Cov(G_x,G_y)/\sqrt{(Var(G_x) * Var(G_y))}$, where G_x and G_y are the genetic effects that influence the two traits x and y. When the two traits are controlled by overlapping genetic factors they will covary, leading to a high genetic correlation value. We applied x-means clustering to the genetic and phenotypic correlation matrices, separately. The x-means algorithm is an iterative form of the k-means clustering algorithm that chooses the best number of clusters, k, using the Bayesian Information Criterion (BIC) [16]. Cluster membership was mapped back onto the 3D surface. Deformation values in the clustered regions were averaged across the cluster. Values in each cluster, for each subject, were used as phenotype values in a GWAS.

Genome-wide association tests were conducted separately within each sample and combined meta-analytically (described below) for the final results. In ADNI and TOP samples, we performed association tests using multiple linear regression, implemented in the *mach2qtl* program [18]. Association tests in the family-based QTIM study employed mixed-effects models to account for twin and family relationships, as implemented in *merlin-offline* [19]. All association tests controlled for sex, age, and intracranial volume (ICV). Each subject's ICV was estimated as the determinant of the affine transformation matrix to the standard FSL template. GWAS results from within each cluster were combined using an inverse variance-weighted meta-analysis, implemented in *metal* [20].

3   Results

Test-retest data show that reproducibility of our hippocampus surface models was moderate but in line with the reproducibility of volume segmentations achieved by others [4] (ICC=0.66 for the left hippocampus and ICC=0.73 for the right) using a low-density icosahedral sampling mesh (called 'icosa2' in SPHARM-MAT) and without smoothing the data (see **Table 1**). We used the most parsimonious model for our analysis; we examined the surface morphology of the 'icosa2' sample surface at 162 vertices (so 324 vertices left and right) with no heat kernel smoothing [17].

Table 1. Intraclass correlation coefficient values for left and right hippocampal surfaces. 'icosaX' is the name of the sampling mesh provided in SPHARM-MAT; larger values in the name represent a finer sampling mesh (more vertices). Heat kernel smoothing was performed at three different standard deviation values (a parameter of the heat kernel smoothing algorithm) for 100 iterations. The most parsimonious model bilaterally uses the 'icosa2' mesh, with no smoothing.

Left Hippo.	No Smoothing	1mm	2mm	3mm
'icosa2'	0.67	0.53	0.53	0.51
'icosa4'	0.67	0.67	0.67	0.67
'icosa6'	0.67	0.67	0.67	0.67
Right Hippo.				
'icosa2'	0.73	0.63	0.62	0.62
'icosa4'	0.73	0.73	0.73	0.73
'icosa6'	0.73	0.73	0.73	0.74

We estimated the number of clusters sufficient to group related vertices based on their phenotypic correlations and separately their genetic correlations with all other points on the hippocampal surface using x-means clustering. The most parsimonious models for both the phenotypic and genotypic correlation matrices determined by BIC were k-means clustering with 2 groups. To visualize the clusters, we mapped the cluster membership back onto the 3D average template surfaces. The cluster memberships determined by the phenotypic correlation are shown in **Fig. 1** and the genotypic correlation in **Fig. 2**. The cluster regions of interest selected by phenotypic correlation are highly similar to those chosen by genotypic correlation. There does seem to be noticeable differences in the cluster membership along the bottom left hippocampal surface. In addition, there was a clear bilateral symmetry, with cluster 1 (*in green*) occupying the outer curves of the structure and cluster 2 (*in red*) the inner curve.
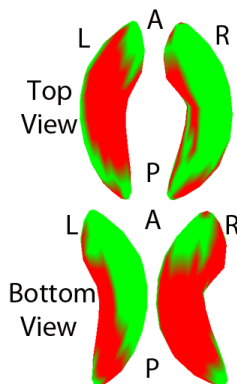

Fig. 1. A 3D projection of the cluster membership determined by phenotypic clustering onto the average template images (*A and P denote anterior and posterior*)
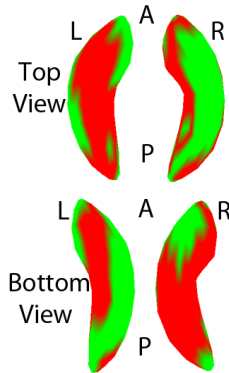
Fig. 2. A 3D projection of the cluster membership from genetic clustering onto the average template images (*A and P denote anterior and posterior*). These are regions where coherent genetic influences are detected, so they are clustered together to provide a coherent signal for GWA.

We conducted a genome-wide association study on the average deformation values in each of the clusters across subjects. Our criterion for significance is the standard genome-wide cut-off ($p<5x10^{-8}$), but after applying a further Bonferroni correction, for testing two separate phenotypes in each condition, our new significance criterion is $p<2.5x10^{-8}$.

After meta-analysis, only cluster 1 from the genetic correlation clustering yielded a region of genome-wide significance. The most strongly associated SNP in the *FBLN2* gene was rs145212527 after meta-analysis: $P_{MA}= 1.25x10^{-8}$; Effect Allele = T; Freq = 0.956; Beta$_{MA}$= 0.354; SE$_{MA}$=0.0621 (**Fig. 3**). Each individual study provided support for this SNP and the same direction of effect (ADNI: p=0.0073, β=0.389, SE=0.145; QTIM: p=0.00059, β=0.300, SE=0.087; TOP: p=0.00017, β=0.421, SE=0.112). Neither of the GWAS analyses of the clusters determined by phenotypic clustering yielded significant results. The top SNP in cluster 1 (rs145212527) was the same SNP found in the genetic clustering analysis of cluster 1. However, the p-value was less strong than for the genetic clustering GWAS and did not pass significance (p=4.6x10^{-7}).
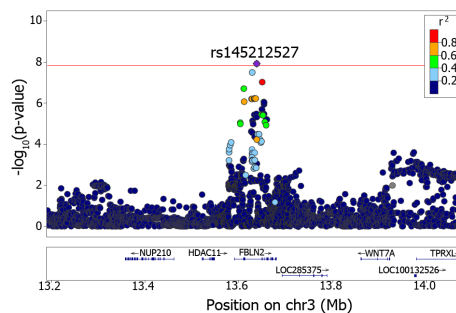

Fig. 3. LocusZoom plot [21] of the most highly associated SNP from the GWAS of cluster 1 from genetic clustering, after meta-analysis. Each point is a SNP; points above the *red horizontal line* are genome-wide significant. Each point's color gives the linkage disequilibrium (r^2) of that point to rs145212527.

4   Discussion

This paper's major contributions are to: 1) perform the first-ever genetic clustering analysis on the hippocampal surface, 2) use genetic correlation values to prioritize and group related regions based on genetic similarity in an image to reduce the multiple comparisons correction, and 3) to demonstrate a case where the added information about common genetic determinants from genetic correlations can boost power for genomic association analyses compared to traditional phenotypic correlation.

In addition, we identified a genome-wide significant SNP affecting hippocampal structure in the *FBLN2* gene. The Allen Human Brain Atlas shows that this gene is differentially expressed in the hippocampus. *FBLN2* is involved with tissue organization, and in differentiation of neurons and other cells [22]. In some ways, clustering the data before performing GWAS is related to performing a GWAS at each point and performing cluster-wise correction for multiple comparisons. The cluster-wise correction methods of Hayasaka and Nichols may be useful for this purpose [23]. However, in this current paper we show that using cluster-wise methods that incorporate genetic correlation methods are more powerful and the methods of [23] do not incorporate genetic correlation into the model. Another paper [24] used sparse models to simultaneously select SNPs from a subset of candidate SNPs and correlated features along the surface. However, the model in [24] has limited utility in high dimensional applications, such as searching the full genome as we did in this study. Additionally, further work is still necessary to confirm that clustering methods are more powerful that voxel-wise analyses. However, this was discussed previously [7]. These are promising findings; further studies will attempt to replicate the genetic results and study the biological pathways they may affect.

References

1. Wang, Y., et al.: Surface-based TBM boosts power to detect disease effects on the brain: An N=804 ADNI study. NeuroImage 56(4), 1993–2010 (2011)
2. Styner, M., et al.: Boundary and medial shape analysis of the hippocampus in schizophrenia. Medical Image Analysis 8(3), 197–203 (2004)
3. Frisoni, G.B., et al.: Mapping local hippocampal changes in Alzheimer's disease and normal ageing with MRI at 3 Tesla. Brain 131(12), 3266–3276 (2008)
4. Stein, J.L., et al.: Identification of common variants associated with human hippo-campal and intracranial volumes. Nature Genetics 44(5), 552–561 (2012)
5. Stein, J.L., et al.: Voxelwise genome-wide association study (vGWAS). NeuroImage 53(3), 1160 (2010)
6. Hibar, D.P., et al.: Voxelwise gene-wide association study (vGeneWAS): multi-variate gene-based association testing in 731 elderly subjects. NeuroImage 56(4), 1875–1891 (2011)
7. Chiang, M.-C., et al.: Gene network effects on brain microstructure and intellectual performance identified in 472 twins. Journal of Neuroscience 32(25), 8732–8745 (2012)
8. Chen, C.-H., et al.: Hierarchical genetic organization of human cortical surface area. Science 335(6076), 1634–1636 (2012)

9. ENIGMA2 Genetics Support Team. ENIGMA2 1KGP Cookbook (v3) (Online). The Enhancing Neuroimaging Genetics through Meta-Analysis (ENIGMA) consortium (July 27, 2012)

10. Patenaude, B., et al.: A Bayesian model of shape and appearance for subcortical brain segmentation. NeuroImage 56(3), 907–922 (2011)

11. Pantel, J., et al.: A new method for the in vivo volumetric measurement of the human hippocampus with high neuroanatomical accuracy. Hippocampus 10(6), 752–758 (2000)

12. Shen, L., Makedon, F.: Spherical mapping for processing of 3D closed sur-faces. Image and Vision Computing 24(7), 743–761 (2006)

13. Brechbuhler, C., Gerig, G., Kubler, O.: Parameterization of closed surfaces for 3D shape description. Comp. Vis. Image Understanding. 61, 154–170 (1995)

14. Shen, L., Farid, H., McPeek, M.A.: Modeling 3-Dimensional Morphological Structures Using Spherical Harmonics. Evolution 63(4), 1003–1016 (2009)

15. Neale, M.C., et al.: Methodology for genetic studies of twins and families, vol. 67. Springer (1992)

16. Pelleg, D., et al.: X-means: Extending k-means with efficient estimation of the number of clusters. In: Proceedings of the Seventeenth International Conference on Machine Learning, vol. 1 (2000)

17. Chung, M.K.: Heat kernel smoothing on unit sphere. In: 3rd IEEE International Symposium on Biomedical Imaging: Nano to Macro. IEEE (2006)

18. Li, Y., et al.: MaCH: using sequence and genotype data to estimate haplotypes and unobserved genotypes. Genetic Epidemiology 34(8), 816–834 (2010)

19. Chen, W.-M., Abecasis, G.R.: Family-based association tests for genomewide association scans. The American Journal of Human Genetics 81(5), 913–926 (2007)

20. Willer, C.J., Li, Y., Abecasis, G.R.: METAL: fast and efficient meta-analysis of genome-wide association scans. Bioinformatics 26(17), 2190–2191 (2010)

21. Pruim, R.J., et al.: LocusZoom: regional visualization of genome-wide association scan results. Bioinformatics 26(18), 2336–2337 (2010)

22. Miosge, N., et al.: The extracellular matrix proteins fibulin-1 and fibulin-2 in the early human embryo. The Histochemical Journal 28(2), 109–116 (1996)

23. Hayasaka, S., Nichols, T.E.: Combining voxel intensity and cluster extent with permutation test framework. Neuroimage 23(1), 54–63 (2004)

24. Wan, J., et al.: Hippocampal surface mapping of genetic risk factors in AD via sparse learning models. In: Fichtinger, G., Martel, A., Peters, T., et al. (eds.) MICCAI 2011, Part II. LNCS, vol. 6892, pp. 376–383. Springer, Heidelberg (2011)